Polar Biol (2008) 31:363–379
DOI 10.1007/s00300-007-0365-0

ORIGINAL PAPER

Optical gradients and phytoplankton production in the Mackenzie River and the coastal Beaufort Sea

Leira Retamal · Sylvia Bonilla · Warwick F. Vincent

Received: 13 March 2007 / Revised: 24 August 2007 / Accepted: 10 September 2007 / Published online: 3 October 2007

Abstract We sampled a 300-km transect along the Mackenzie River and its associated coastal shelf system (western Canadian Arctic) in July–August of 2004 to evaluate the gradients in optical, phytoplankton and photosynthetic characteristics. The attenuation of photosynthetically available radiation (PAR) was best explained by coloured dissolved organic matter (CDOM) and turbidity (non-algal particles), while UV attenuation correlated most strongly with CDOM. Bacillariophyceae and Chlorophyceae dominated in the river, and shifted to Cryptophyceae and Prasinophyceae in the estuarine transition zone. In the coastal shelf waters, picoplanktonic cells dominated the surface autotrophic communities while both large and small cells occurred in the deep chlorophyll maximum. High PAR attenuation reduced the integral primary production rate in the river, while at an offshore marine site, 55% of integral production was at or below the pycnocline, under low PAR. Climate change is likely to increase the sediment and CDOM loading to these waters, which would exacerbate light limitation of photosynthesis throughout the system.

L. Retamal (✉) · W. F. Vincent
Centre d'Études Nordiques & Département de Biologie,
Laval University, Quebec City, QC, Canada G1K 7P4
e-mail: leira.retamal.1@ulaval.ca

S. Bonilla
Facultad de Ciencias, Universidad de la República,
Montevideo 11400, Uruguay

Present Address:
L. Retamal
Institut National de la Recherche Scientifique Eau,
Terre et Environnement, Quebec City, QC, Canada G1K 9P9

Keywords Arctic · Beaufort Sea · Estuary · Light · Optics · Phytoplankton · Primary production · River

Introduction

The Arctic Ocean is strongly influenced by river inflows. Global circulation models predict major changes in the arctic climate over the course of this century that will likely affect all river discharges and their sediment and solute loads into the Arctic Ocean (Dittmar and Kattner 2003; Hill and Cota 2005). These changes in inflow dynamics are likely to have a pronounced impact on the physical and chemical properties of coastal shelf ecosystems, which currently support more than 80% of the total primary production in arctic seas (Platt et al. 1987; Hill and Cota 2005).

Primary production in the Arctic is constrained to a period of less than 150 days per year and is strongly regulated by light availability and nutrients, especially nitrate and silica (Gosselin et al. 1997; Carmack and MacDonald 2002; Millot et al. 2003; Carmack et al. 2004). Phytoplankton dynamics in arctic coastal waters are likely to be influenced by the sediments, nutrients and biota entering from rivers (Matishov et al. 2001; Trefry et al. 2005; Waleron et al. 2007). Arctic coastal regions are also characterized by strong salinity stratification and complex nearshore dynamics associated with the mixing of water masses with different oceanographic properties, and this habitat complexity in turn affects the organisation of their phytoplankton communities (Wehr and Descy 1998; Manson et al. 2001).

Unlike lower order rivers, large rivers support a well-developed phytoplankton community that builds up over the days to weeks of transit from their source waters to the sea (WRI 2003). Little is known, however, about the phytoplankton characteristics of large arctic rivers despite

their total water volume and the vast distances over which they flow. Most of these rivers have their source waters in the subarctic or higher latitudes of the north temperate zone, more than 1,000 km from their discharge point into the Arctic Ocean. The rivers may be highly turbid, such as the Mackenzie River, and may also contain high concentrations of coloured dissolved organic matter (CDOM), for example the Lena River that is referred to as a 'black water system' (Gibson et al. 2000). These optically active constituents are likely to exert a strong control on underwater light availability in the river and coastal shelf environment, and thereby influence the photosynthetic characteristics of the river and estuarine phytoplankton. Sediment and CDOM concentrations are expected to increase commensurate with permafrost melting under a warmer climate regime (ACIA 2005), and there is a need for an improved understanding of how these changes may impact on primary production.

In the present study, we had three objectives. Firstly, we aimed to describe the hydrologic optics of the Mackenzie River and its associated estuary, with emphasis on determining the factors that control underwater photosynthetically active radiation (PAR, 400–700 nm) and ultraviolet radiation (UVR, solar radiation <400 nm). Although such data are particularly sparse for arctic waters, the optical regimes of large rivers are poorly characterized at all latitudes despite the economic and ecological importance of these systems, and the fundamental role of underwater radiation in modulating primary production and photochemical activities. Secondly, to address the lack of knowledge concerning arctic river phytoplankton, we analysed the algal pigment composition in the river and estuary by fractionation and high performance liquid chromatography (HPLC) to identify changes in size and taxonomic structure across the transition from freshwater to saltwater. Finally, to further evaluate the relationships between algal community processes and the downstream gradient in environmental properties we assessed the spatial variations in PAR absorption and photosynthesis by the phytoplankton. This study was undertaken within the program Arctic River Delta Experiment (ARDEX), during the period of coastal open water conditions and was by way of a 300 km long transect, from upstream freshwater sites on the Mackenzie River, across its estuary and into the coastal Beaufort Sea.

Materials and methods

Study site

The Mackenzie River is the longest river in Canada and extends 1,600 km from Great Slave Lake (61°N, 115°W), to the Arctic Ocean (69°N, 135 °W). It drains 1.707×10^6 km^2 and is fed by many tributaries from the subarctic and arctic regions of Northwest Territories (Millot et al. 2003; RNC 2003). Large parts of north basin have permanent permafrost even in the sediments of the submerged delta (Millot et al. 2003; RNC 2003). The vegetation cover is mainly composed of boreal forest in the northwest, with tundra in the extreme northeast of the catchment, and deciduous forest, riparian spruce and abundant thermokarst lakes and peatland in the central part of the catchment (Telang et al. 1991; Yunker et al. 1995; Droppo et al. 1998). The Mackenzie River is estimated to deliver 2.65×10^6 t of dissolved organic carbon (DOC) into the Beaufort Sea each year (Telang et al. 1991), and is the highest ranking of all arctic rivers in terms of the amount of POM delivered to the Arctic Ocean (Knap et al. 1996).

Sampling

The ARDEX sampling cruise was undertaken from 26 July to 2 August 2004 beginning in the East Channel at Inuvik (station R1), 250 km upstream from the river mouth. Sampling continued down the East then Middle Channel (stations R2–R4), extended into the estuarine transition zone (ETZ, the transition from freshwater to saltwater; stations R5d and R5a) and then out over the Mackenzie Shelf, stations R6 (a CTD station only), R7, R8 and R9 (Fig. 1). The outermost station R9 was at the same coordinates as the innermost station sampled during the Canada Arctic Shelf Exchange Study (CASES 2002 Station 65, as in Garneau et al. 2006). All ten stations were sampled at the surface and bottom, as well as within the deep chlorophyll

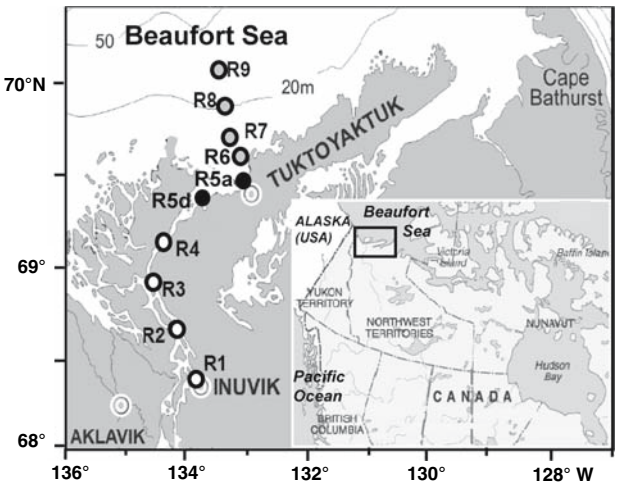

Fig. 1 Sampling sites on the Mackenzie River, estuarine transition zone (*ETZ*) and coastal shelf during the ARDEX program in the western Canadian Arctic, July–August 2004. The *open circles* show the position of the river stations (R1–R4), *black-filled circles* show the estuarine transition zone stations (R5d, a) and *grey-filled circles* show the coastal shelf stations (R6–R9)

a maximum wherever this feature was detected during the CTD profiling. Surface samples were collected with a 15 l bucket or by a subsurface continuous pump, and deeper samples were collected with an opaque, 6.2 l Kemmerer bottle. Water column profiles of temperature, salinity, and Chl *a* were acquired with a CTD profiling logger (RBR Inc., Canada) coupled with a Wetstar fluorometer (WetLabs Inc., USA).

Chemical analyses

Dissolved inorganic carbon (DIC) concentrations were measured in 40 ml of non-filtered water samples and analyzed on board the ship within 1–2 h of collection. Samples were maintained at in situ temperature in air-tight BOD bottles until analysis. Alkalinity and DIC concentrations were obtained by semi-automatic titration with 0.2 N H_2SO_4 (Sharp et al. 1993; Knap et al. 1996). Dissolved organic carbon (DOC) samples were filtered through 0.2 µm Nuclepore membrane filters and the filtrate then stored in air-tight acid-washed, sample-washed, amber bottles (120 ml for DOC and 250 ml for CDOM absorption) in the dark at 4°C for up to 2 months until further analysis. These samples were also to be used for synchronous fluorescence analysis and we therefore avoided adjusting the pH or freezing them to prevent fluorescence changes (Belzile et al. 2002; Pullin and Cabaniss 1995). DOC concentrations were obtained by high temperature oxidation using a Shimadzu TOC Analyzer 5000A with detection limits of 0.05 mg l^{-1}. Before analysis, the samples were acidified with 0.01 N HCl to a final pH of 2.0 and then bubbled with CO_2-free nitrogen for 7 min to ensure the removal of all DIC, as recommended for high DIC water (Sharp et al. 1993; Knap et al. 1996). Dissolved organic nitrogen (DON) values for the estimation of ratios were obtained from Emmerton (2006).

Seston analysis

Turbidity was measured in the samples immediately after collection in nephelometric turbidity units (NTU) using an Aquafluo handheld nephelometer (Turner Designs Inc., USA). Samples for total suspended particulate matter (SPM) were filtered onto pre-combusted (500°C) Whatman GF/F (0.7 µm) pre-weighed glass fibre filters, with sufficient measured volumes of water until total clogging of the filter. The filters were then dried at 60°C and re-weighed for total SPM, after which they were combusted at 500°C to determine the total inorganic and organic (by difference) fractions. Additional samples were filtered onto pre-combusted GF/C (pore size 1.2 µm) 25 mm diameter glass fibre filters and stored frozen until analysis for particulate organic carbon (POC) and nitrogen (PON). This analysis was by high temperature oxidation using a LECO CHNS-932 elemental analyzer, which had a detection limit of 0.03 mg l^{-1} for carbon and 0.005 mg l^{-1} for nitrogen. The filters were acidified by HCl-fuming overnight and allowed to dry at 65°C prior to analysis in tin or silver sleeves.

Pigment analysis by HPLC

Phytoplankton samples of 500 to 2,000 ml were filtered onto 25 mm diameter GF/F glass fibre filters, before (total phytoplankton) or after (the <3 µm picophytoplankton fraction) filtration through a Poretics polycarbonate filter (47 mm diameter, 3 µm pore size). Filters were stored frozen onboard the ship at –80°C in the dark until sonication in 3 ml of 95% methanol. The extracts were then cleared by centrifugation (10 min, 4,000 rpm) and filtrated through 0.2 µm Acrodisc filters. They were stored under Argon gas at 4°C in darkness and then analyzed within 24 h of extraction; 100 µl of the phytoplankton extracts were injected into a Varian ProStar HPLC (Varian Inc., Mulgrave, Australia) equipped with a Symmetry C8 column (4.6 × 150 mm, 3.5 µm pore size; Waters Corporation, Milford, MA, USA). The pigment peaks were detected by diode-array spectroscopy (350–750 nm) set to a slit width of 1 nm. Absorbance chromatograms were obtained at 440 nm (for chlorophylls) and 450 nm (for carotenoids). Chlorophylls were also detected by fluorescence (Ex/Em: 440/650 nm). Standards for identification and quantification of pigments (chlorophyll *a*, *b* c_1, c_2, c_3 and β,β-carotene, echinenone, lutein, alloxanthin, fucoxanthin, violaxanthin, diadinoxanthin, zeaxanthin) were obtained from commercial sources (Sigma Inc., St Louis, MO, USA, and DHI Water & Environment, Hørsholm, Denmark) to calibrate the HPLC. The MgDVP and prasinoxanthin peaks were identified with a derived standard from a culture of *Micromonas pusilla* and areas were converted to concentrations. The HPLC solvent protocol followed the procedure of Zapata et al. (2000) based on the heterocratic delivery of two solvent mixtures: a methanol:acetonitrile:aqueous pyridine (50:25:25 v:v:v) solution, and a methanol:acetonitrile:acetone (20:60:20 v:v:v) solution. The flow rate was set to 1 ml min^{-1} and the equilibration time to 7 min.

Underwater irradiance profiles

Integrated PAR and four UVR wavebands (380, 340, 320 and 308 nm) were recorded with a PUV-500 radiometer (Biospherical, CA, USA). The radiometer was deployed from a derrick on the sunlit side of the ship to avoid shadow

effects, and was lowered at slow and constant speed. Diffuse attenuation coefficients $K_{d(\lambda)}$ were determined for all data in the upper water column where our graphical analysis showed there was an exponential decrease in irradiance; the maximum depth limit for this calculation varied according to wavelength. The coefficients were computed from linear regressions of the natural log of downwelling irradiance as a function of depth using SigmaPlot 9.0.

CDOM absorption

CDOM samples from the DOC filtrate were measured in acid-cleaned 10 cm quartz cells using a Varian Cary Bio 300 scanning spectrophotometer. Samples were scanned at 1 nm intervals between 200 and 850 nm, against MilliQ pure water. The spectrum was corrected for the absorption offset using the mean value for wavelengths greater than 800 nm. The absorption coefficients were calculated as:

$$a_{\mathrm{CDOM}}(\lambda) = 2.303 \times A(\lambda)/L$$

where A (λ) is the optical density for wavelength λ and L is the cell path length in m. The CDOM properties were fitted by nonlinear regression from 300 and 650 nm to the equation:

$$a_{\mathrm{CDOM}}(\lambda) = a_{320} \times \exp[S(320 - \lambda)]$$

where a_{320} is the absorption coefficient at 320 nm and S is the slope of the fitted curve (exp refers to the natural base e). The value of a_{320} provides a quantitative estimate of CDOM concentration, while the S-values provide a measure of qualitative variation.

In vivo absorbance

For phytoplankton absorption, 50 to 300 ml of samples were filtered through 0.7 µm GF/F Whatman glass fibre filters using a fritted glass support (25 mm/funnel of 500 ml). The filters were stored frozen at –80°C inside a tissue basket until analysis. All filters, including the blanks, were from the same box to minimize fiber filter variations. The absorbance scans were made with a Cary Bio 300 scanning spectrophotometer (Varian Co., Australia) equipped with an integrating sphere (Labsphere Inc., NH, USA). The scans were corrected for scattering and pathlength amplification according to Mitchell et al. (2003). Phytoplankton absorption (a_{ph}) was determined as the difference between total particle absorption (a_{p}) and absorption by nonalgal particles (a_{NAP}), the latter obtained by scans of the same filter after methanol extraction as in Kishino et al. (1985) and Mitchell et al. (2003). The a_{ph} values were normalized to Chl a concentrations to give specific absorption (a^*_{ph}).

Primary production

Photosynthesis versus irradiance (P–E) curves were obtained using the Rae-box incubation system (Rae and Vincent 1998). The incubations were performed under natural light on the deck of the ship in water-containing boxes in which the temperature was controlled to within 1°C of the temperature measured at the depth of sampling. The Rae-boxes allowed duplicate borosilicate (which reduces short-wavelength UV radiation) scintillation vials containing water samples to be incubated under 11 different neutral shading screens giving 100, 66, 40, 39, 38, 27, 15, 5, 4.8, 4.5 and 3.7% of incident irradiance (400–700 nm). The irradiance at each position in the incubator was measured with a 4π quantum irradiance probe (Biospherical Inc., CA, USA). The probe was submerged inside the scintillation vial with the same volume of sample used for the incubation. Additional vials were wrapped in aluminum foil to measure dark fixation. The incubations were run for surface waters for 60–90 min, and at two marine stations P versus E curves were also determined for samples from the deep chlorophyll maximum. Each sample of 20 ml was inoculated with [^{14}C]-HCO_3^- to a final concentration of 0.2 µCi ml^{-1}. Counts were obtained using a Beckman LS6500 liquid scintillation counter and were transformed to rates of carbon fixation using the JGOFS algorithm (Knap et al. 1996). Carbon fixation data were normalised to Chl a and fitted to the equation of Platt et al. (1980) using an iterative non-linear regression (SigmaPlot 9.0):

$$P^* = P^*_{\mathrm{s}} \times [1 - \exp(-\alpha E/P^*_{\mathrm{s}})] \times [\exp(-\beta E/P^*_{\mathrm{s}})]$$

where P^* is photosynthesis normalised to Chl a at irradiance E, P^*_{s} is the photosynthetic rate in the absence of photoinhibition, α is the light utilisation coefficient and β is the photoinhibition parameter. The maximum photosynthetic rate was calculated as in Platt et al. (1980):

$$P^*_{\mathrm{max}} = P^*_{\mathrm{s}} \times [\alpha/(\alpha + \beta)] \times [\beta/(\alpha + \beta)]^{\beta/\alpha}$$

The photosynthetic parameters P^*_{s}, α and β (were then used to calculate P at a depth intervals of 0.1 m in the river and ETZ and 0.25 m at each station offshore as

$$P(z)^* = P^*_{\mathrm{s}} \times [1 - \exp(-\alpha E_{\mathrm{d}}(z)/P^*_{\mathrm{s}})] \times [\exp(-\beta E_{\mathrm{d}}(z)/P^*_{\mathrm{s}})]$$

$E_{\mathrm{d}}(z)$ is the downwelling PAR irradiance at depth (z) calculated according to the diffuse attenuation coefficient (K_{dPAR}):

$$E_{\mathrm{d}}(z) = E_{\mathrm{d0-}} \times \exp(-K_{\mathrm{dPAR}} \times z)$$

where $E_{\mathrm{d0-}}$ is the PAR irradiance just below the water surface. The shape of the daily irradiance curve was

determined from the geographical position, period of the year and solar angle (Oke 1988) for each station, and each of these curves was adjusted to measured values of E_{d0-} at the time of sampling. These irradiance curves were then averaged to calculate integrated daily primary production under the same surface irradiance conditions for all stations. For the coastal shelf site, integral production in mg C m^{-1} day^{-1} was calculated separately for above and below the pycnocline using the surface and deep water photosynthetic parameters and the fluorescence profile of Chl *a*. The daily integrated primary production rates were calculated for time steps of 1 h and for depth intervals of 0.1 m (river and ETZ) or 0.25 m (offshore), and these were then integrated through time and depth by Simpson's integration.

Statistical analysis

Descriptive statistics, one way ANOVA, regression and correlation analyses were made using SigmaStat 3.1 and SigmaPlot 9.01 (Systat Software, Inc.). Average values were calculated for each of the three regions of the Mackenzie system (river, transition zone and offshore) and the values in parentheses for each mean are ±SD. Multiple linear regressions were conducted on non-covariant variables, and the significance level was set at 95% for all analyses.

Results

Water column structure

The Mackenzie River had a homogenous, well-mixed water column throughout the freshwater reach of the transect (Table 1). Water temperatures at the river stations were 17–19°C, with a salinity of 0.13 psu (Fig. 2a). Surface temperatures dropped across the estuary to 14°C, and despite the shallow depth at these stations (2–4 m), the water columns were stratified, with 1°C cooler water beneath the halocline situated at 2 m (R5d) and 1.7 m depth (R5a). Surface temperatures decreased offshore to a minimum of 8°C at R9. At this station the surface layer was still strongly influenced by the river (surface salinity at R9 of 25.22 psu) and was separated by a strong halocline at

Table 1 Station characteristics along the ARDEX cruise transect from the river, estuarine transition zone (ETZ) and shelf zones

Station	Date	Latitude (°N)	Longitude (°W)	Z_{max} (m)	Z_p (m)	Z_s (m)	Z_{eu} (m)	Z_{320}/Z_{eu} (%)	Z (m)	pH	DOC (g m^{-3})	DIC (g m^{-3})
River												
R1	26–07	68.38	132.25	2.6	*F*	0.2	0.8	16	0	8.34	4.8	25.68
R2	02–08	68.60	134.20	21.4	*F*	0.3	1.1	34	0	8.55	3.2	25.86
									20	8.48	3.2	26.94
R3	01–08	68.88	134.57	29.6	*F*	0.3	1.0	29	0	8.41	3.4	28.02
									26	8.35	3.7	24.48
R4	27–07	68.20	134.23	18.9	*F*	0.2	0.7	41	0	8.46	3.8	25.44
									6	8.40	3.6	24.84
Estuarine transition zone												
R5d	31–07	69.38	133.83	3.7	2.0	0.3	0.8	41	0	8.45	3.4	24.90
									3.5	*NS*	3.1	*NS*
R5a	31–07	69.38	133.83	2.9	1.7	0.7	2.1	39	0	8.45	4.9	26.46
									2.5	8.30	2.8	28.20
Shelf												
R6	30–07	69.55	133.40	*NS*	*NS*	0.7	*NS*	*NS*	0	*NS*	*NS*	*NS*
R7	30–07	69.72	133.42	7.4	5.0	2.4	5.0	24	0	*NS*	2.7	*NS*
									6.5	*NS*	1.8	*NS*
R8	30–07	69.88	133.42	15.9	7.0	9.9	16.9	17	0	8.37	2.8	31.14
									12[a]	8.21	1.3	31.14
R9	28–07	70.05	133.42	31.8	5.0	14	14.9	16	0	8.35	2.2	32.28
									15	*NS*	2.3	*NS*
									21[a]	8.18	1.5	31.80

Z_{max}: maximum depth, Z_p: depth of pycnocline, Z_s: Secchi depth, Z_{eu}: depth limit of the euphotic layer calculated as 1% of incident irradiance using K_{dPAR} values, Z_{320}/Z_{eu}: percentage of the euphotic layer affected by UVR (depth of 10% of surface 320 nm UVR relative to 1 % of surface PAR), *Z*: sampling depth, *DOC* dissolved organic carbon, *DIC* dissolved inorganic carbon, *F* fully mixed water column, *NS* not sampled

[a] Deep chl *a*

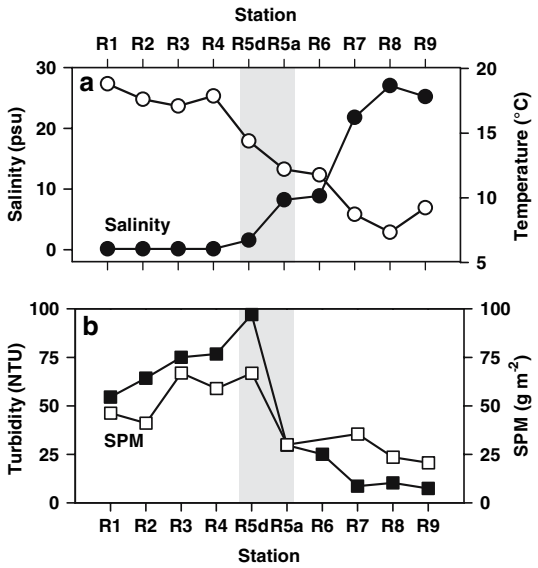

Fig. 2 Surface water properties along the ARDEX transect: **a** salinity (*black-filled circles*) and temperature (*white-filled circles*); **b** turbidity (*black squares*) SPM (*white squares*). The *grey zone* indicates the estuarine transition zone

5–7 m from the deeper marine waters that had temperatures below 0°C at 15 m and salinities above 31.06 psu. There was no significant variation in surface pH values across the transect, from a mean (±SD) of 8.5 ± 0.1 in the river, to 8.4 ± 0.1 in the estuary and 8.3 ± 0.1 offshore (Table 1).

Dissolved inorganic and organic carbon

DIC concentrations in the river averaged 25.9 ± 1.1 g m^{-3} increasing to 26.3 ± 1.5 g m^{-3} in the estuary and to 31.7 ± 0.6 g m^{-3} at the shelf stations (Table 1). One way ANOVA showed that there was a significant difference in DIC between the shelf region and the river and estuary sites ($F = 29.63$; $df = 14$; $P < 0.001$). DOC concentrations were similar in the river and estuary with mean values of 3.6 ± 0.5 and 3.6 ± 0.8 g m^{-3} respectively, and dropping to 2.1 ± 0.6 g m^{-3} offshore, and as for the DIC there was a significant difference between the freshwater influenced regions and the shelf ($F = 13.99$; $df = 20$; $P < 0.001$). The DOC/DON ratio dropped substantially from a mean value of 68 ± 20 in freshwater, to 31 ± 15 in the estuary and 8 ± 3 over the shelf, with significant differences among the three regions ($F = 46.55$; $df = 20$; $P < 0.001$).

Seston

The concentrations of total suspended matter were high at all river stations and then decreased across the estuarine transition zone (Fig. 2b). There was a close correspondence between the laboratory-derived SPM values and the nephelometric turbidity values measured in the field (Fig. 2b), according to the equation NTU = 1.7·SPM –29.4 ($r = 0.92$; $F = 40.10$; $P = 0.0004$). The seston was mostly composed of inorganic materials, with an organic content of less than 12% of the total SPM in the river and the estuary samples, increasing slightly to 14% offshore. The mean concentrations of particulate organic carbon were 1.3 ± 0.3 (river), 1.0 ± 0.6 (estuary) and 0.5 ± 0.7 (shelf) g m^{-3}. The particulate organic nitrogen dropped from mean values of 0.20 ± 0.08, to 0.10 ± 0.02 to 0.05 ± 0.07 g m^{-3} over the same sequence. The POC/PON ratio differed greatly from the dissolved ratios, with mean values of 11 ± 4 in the river, 9 ± 4 in the estuary stations and 11 ± 6 in the shelf, with no significant differences among the three groups of stations ($F = 0.64$; $df = 20$; $P = 0.54$). The ratio of DOC to POC increased from mean value of 2.8 ± 0.5; to 4.9 ± 2.9 to 13.3 ± 13.3, but these differences were not significant ($F = 1.99$; $df = 20$; $P = 0.16$) given the high within-group variances. The DON/PON ratios differed significantly among the three groups ($F = 30.51$; $df = 21$; $P < 0.001$), from 0.5 ± 0.3 for the river stations, to 1.2 ± 0.6 for the estuary and 17.6 ± 10.9 for the offshore sites.

Underwater irradiance

There were striking changes in the underwater light regime across the transect, with Secchi depth values that ranged from a minimum of 0.2 m in the river to 14 m in the offshore ocean (Table 1). The river was turbid at all freshwater sampling stations, with PAR attenuation coefficients (K_{dPAR}) that were consistently high, averaging 5.2 ± 1 m^{-1} (Fig. 3a). There was an abrupt increase in transparency across the estuary, with K_{dPAR} dropping from 5.4 at R5d to 2.2 m^{-1} at R5a. The offshore waters had the greatest transparency, with K_{dPAR} values averaging 0.5 ± 0.4 m^{-1}, an order of magnitude lower than in the river (Fig. 3a).

The K_{dPAR} values were strongly correlated with a_{320} ($r = 0.89$, $P = 0.001$) and to a slightly lesser extent with turbidity ($r = 0.84$, $P = 0.004$). There was no correlation between a_{320} and turbidity, and a multiple linear regression of K_{dPAR} against both variables was highly significant ($r = 0.93$, $P < 0.001$). The deep maximum Chl *a* was at 0.24% of the incident surface PAR irradiance at station R7, 3.8% at R8 and 0.15% at station R9.

The attenuation coefficients for UVR at 320, 340 and 380 nm were generally high (Fig. 3b) and correlated strongly with a_{320} throughout the transect (for K_{d320}: $r = 0.92$, $P = 0.001$; K_{d340}: $r = 0.95$, $P < 0.001$; K_{d380}: $r = 0.96$, $P < 0.001$). There was no correlation between

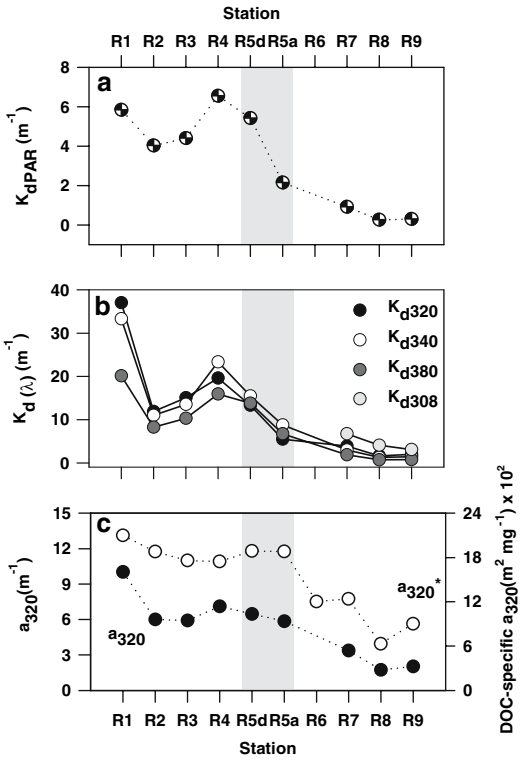

Fig. 3 Optical parameters at each ARDEX station: **a** diffuse attenuation coefficient for PAR; **b** diffuse attenuation coefficients for UV radiation at 320, 340, 380 and 308 nm; **c** CDOM absorption at 320 nm (a_{320} *black-filled circles*) and DOC-specific a_{320} (a^{*}_{320} *white-filled circles*)

K_{d320} or K_{d340} and turbidity alone (K_{d320}:$r = 0.5$, $P = 0.17$; K_{d340}: $r = 0.63$, $P = 0.1$) or Chl *a* (K_{d320}: $r = 0.13$, $P = 0.75$; K_{d340} $r = 0.2$, $P = 0.60$). The goodness-of-fit was higher when predicting the UVR attenuation coefficients by a multiple linear regression with a_{320} and turbidity (K_{d320}: $r = 0.98$, $P < 0.001$; K_{d340}: $r = 0.97$, $P < 0.001$), however only the variable a_{320} was significant ($P < 0.05$) in this regression. In contrast with shorter wavelength attenuation, K_{d380} was significantly correlated with turbidity ($r = 0.77$, $P < 0.02$), and as for PAR the best fit was a multiple linear regression on both CDOM and turbidity ($r = 0.98$, $F = 49.75$; $P < 0.001$), with both variables significant ($P < 0.05$). The shortest wavelength UVR (308 nm) recorded by our instrument was attenuated very rapidly in the river and ETZ, and K_{d308} values could only be estimated over the shelf stations; for this limited data set there was no significant correlation with a_{320} ($n = 3$; $r = 0.90$; $P = 0.28$).

Absorption coefficients

CDOM concentrations as measured by a_{320} showed a general decrease over the transect (Fig. 3c). These values were a linear function of salinity indicating their conservative behavior across the freshwater–saltwater transition at this time of year ($r = –0.89$; $P = 0.001$). There was a linear correlation between DOC and CDOM ($r = 0.81$, $P = 0.008$). However, DOC was not correlated with salinity ($r = –0.64$, $P = 0.06$), indicating a mixing of coloured and uncoloured dissolved organic materials. On the other hand, DOC-specific a_{320} (a^{*}_{320}) decreased over the offshore transect (Fig. 3c) and correlated with salinity to a greater extent than a_{320} ($r = –0.9$, $P = 0.0003$). The *S*-values were between 0.0183 and 0.0187 nm^{-1} and no significant differences were found over the three sections of the Mackenzie River-Shelf system (ANOVA $P = 0.25$). CDOM absorption was a major component of total PAR absorption at most stations (Fig. 4a–d). In the river and estuary its contribution ranged from 27% at R1 to 21% at the R4 (Fig. 5). Higher contributions were recorded in the marine waters, from 31% at R5a to 44% at R7 and 41% at R9.

The phytoplankton contribution to total underwater absorption (integrated over the PAR range 400–700 nm) in

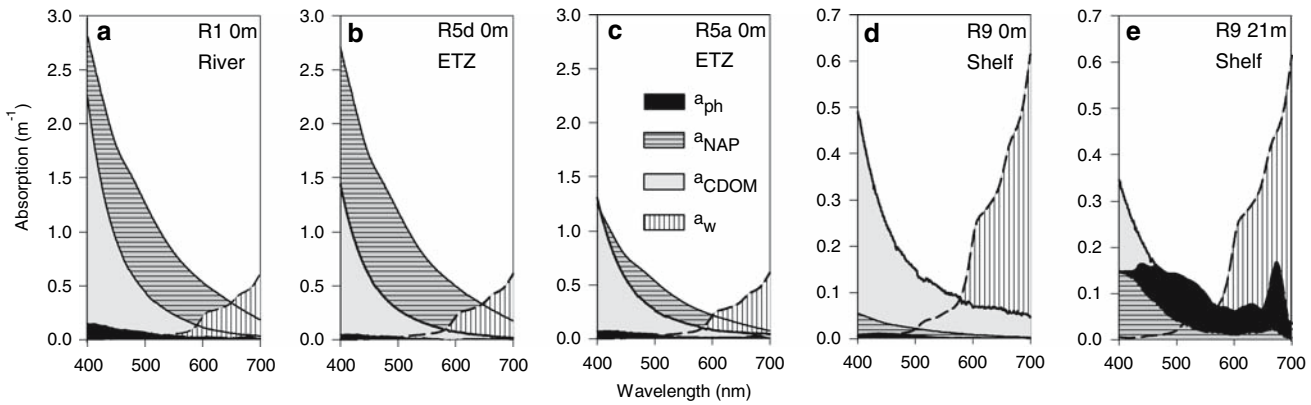

Fig. 4 Spectral absorption by phytoplankton (a_{ph}), nonalgal particles (a_{NAP}), CDOM (a_{CDOM}) and water (a_{W}) in each of the three sections of the Mackenzie estuarine system

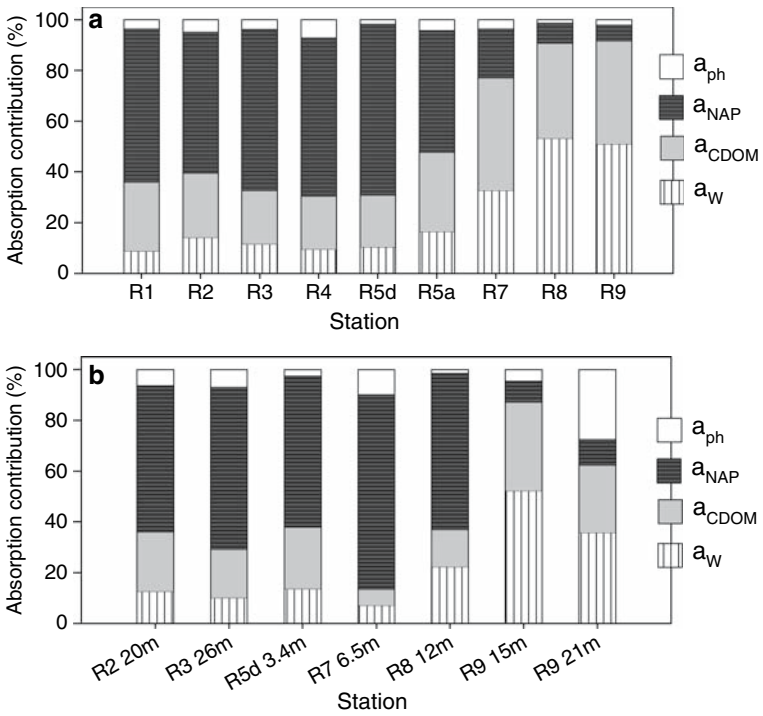

Fig. 5 Percent contribution by each optically active component to total PAR absorption: phytoplankton (a_{ph}), nonalgal particle (a_{NAP}), CDOM (a_{CDOM}) and water (a_W). **a** surface waters; **b** deep waters

the surface waters ranged from 4% at R1 to 7% at R4 (Fig. 5). The a_{ph} contribution in the estuary was lower than in the river with 2% at R5d 0 m. Although they had similar spectral shapes, R5d 3.4 m and R5a 0 m differed in their contribution to total absorption, with 2 and 4%, respectively. Over the shelf, the phytoplankton contribution varied among stations, with the greatest contribution in the deep samples (Fig. 5). In the furthest offshore station (R9), the phytoplankton contribution to total underwater absorption increased by a factor of 14 from the surface to bottom (Fig. 4d, e). When normalized to Chl *a* (a^*_{ph}) the spectral absorption curves were generally similar in each region, but with stronger absorption in the river relative to the estuary and offshore sites (Fig. 6a–c). Two notable exceptions to this trend were the curves for the deep phytoplankton at R7 and R9 (Fig. 6d). Specific absorption by the phytoplankton was always greatest at 440 nm (Fig. 7) and there was a positive exponential relationship between a^*_{ph} and K_{dPAR} ($a^*_{ph}(440)$: $r = 0.94$, $P = 0.001$; $a^*_{ph}(550)$: $r = 0.91$, $P = 0.005$). The shape of the a^*_{ph} spectra was unusual relative to typical oceanic curves, where there is a decrease in absorption before the 440 nm peak (e.g., Ficek et al. 2004; Bricaud et al. 1995), and may reflect a large input of lipid-soluble, pigmented compounds from terrestrial sources.

The absorption due to non-algal particles a_{NAP}, was high throughout the river (>55%), and dropped across the transition zone to lowest values over the shelf, indicating the gradual loss or dilution of riverine particles (Fig. 5). Two deep marine samples had high NAP contributions: at R7 6.5 m, where a_{NAP} contributed 77% of total PAR absorption, likely resulting from tidal mixing and strong sediment resuspension in these shallow waters, and at R8, 12 m, where NAP was more likely derived from phytoplankton detritus and a_{NAP} contributed 62% of the total absorption (Fig. 5).

The contribution of absorption by water itself a_w, to total absorption varied greatly among sites (Figs. 4, 5). For the surface waters, a_w contributed around 11% of total absorption in the river, increasing to 17% at R5a and 50% offshore. For the deep samples, the contribution of a_w ranged from 7% at R7 to 36% at R9.

HPLC pigment analysis

Chl *a* concentrations in the river ranged from 0.6 (R4) to 1.6 (R2) mg m^{-3} with no statistical differences between surface and bottom samples ($t = 0.73$, $df = 5$, $P = 0.50$). In the estuary, values ranged from 0.73 (R5d) to 1.9 mg m^{-3} (R5a). Significantly lower values ($t = 3.17$, $df = 5$, $P = 0.025$) were recorded in the surface offshore waters, from 0.13 (R9) to 0.45 mg m^{-3} (R7), with an order of magnitude higher concentration of 2.2 mg m^{-3} in the deep chl *a* maximum at R8 (Table 2). The DOC specific a_{320} values (a^*_{320}) were not correlated with Chl *a* ($r = -0.7$, $P = 0.06$).

The picoplankton fraction made only a small contribution to Chl *a* stocks at the river stations (1–6%), increasing to 7–20% in the estuarine transition zone (Table 2). In

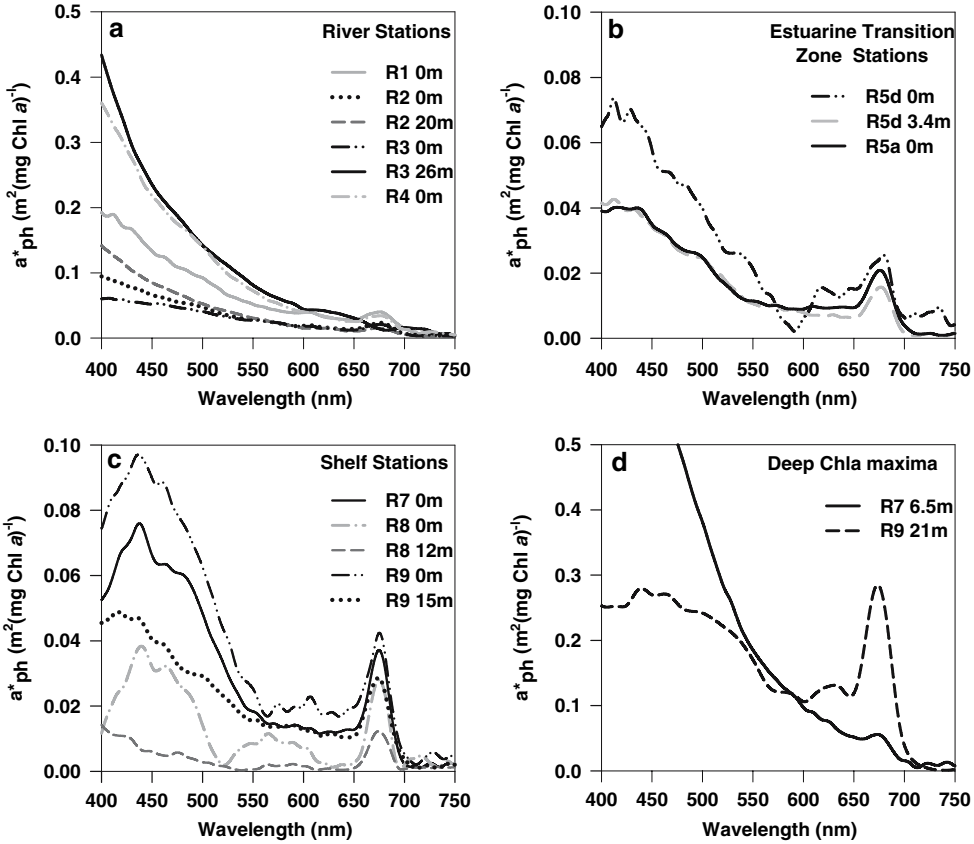

Fig. 6 Phytoplankton-specific absorption spectra for samples from: **a** the river; **b** the estuarine transition zone (ETZ); **c** coastal shelf stations; and **d** deep Chl *a* maxima

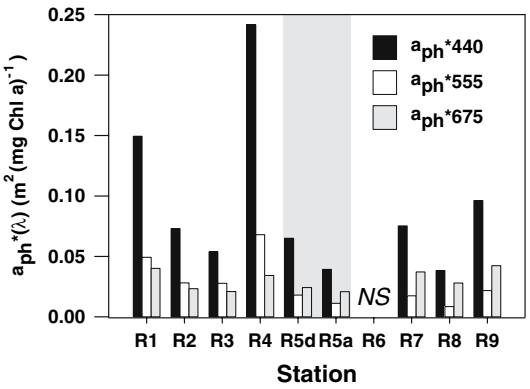

Fig. 7 Phytoplankton-specific absorption (a^*_{ph}) at 440, 555 and 675 nm over the ARDEX transect. *NS* not sampled

contrast, this fraction dominated the offshore phytoplankton, with a contribution from 61 to 77% of the total Chl *a* (Table 2). The ratio of total carotenoids to Chl *a* (weight ratio) was around 1.0 in the river and the estuary with no vertical differences (Table 2). These ratios decreased to a mean value of 0.5 in the offshore surface waters, while the deep samples exceeded 1.4.

All of the measured accessory pigments were normalized to total Chl *a* to facilitate the analysis of compositional changes (Table 2). The pigment signatures of the river samples indicated a community represented by Bacillariophyceae, Raphidophyceae and probably another fucoxanthin groups (chlorophylls c_1 and c_2; fucoxanthin, diadinoxanthin) and Chlorophyceae (Chl *b*, lutein, zeaxanthin), Cyanobacteria (zeaxanthin, although this may also have been from the Chlorophytes) and Cryptophyceae (Chl c_2, alloxanthin) (Table 2). Chl c_3, a diagnostic pigment of the Prymnesiophyceae and Chrysophyceae was detected only at trace levels at these sites, as was echinenone, indicative of picocyanobacteria. MgDVP occurred at the outer estuarine site R5a, suggested the presence of Prasinophyceae (Table 2).

Pigments indicative of Bacillariophyceae and Cryptophyceae were measured over the shelf (Table 2). The relative contribution of Chl c_2 was very low in the River and increased from the ETZ all through the offshore. Chl *b* and zeaxanthin were also present, but the gradual decrease in the Chlorophyceaen pigments lutein and violaxanthin suggest a shift in green algal composition or physiology. The <3 μm fraction contained MgDVP and prasinoxanthin, suggesting the importance of picoprasinophytes at these sites (Table 2). Measurable Chl c_3 concentrations at the shelf stations indicated the presence of Prymnesiophytes or Chrysophytes (R8 0 m: 0.25 mg m^{-3}, 24% contribution from <3 μm; R9 0 m: 0.16 mg m^{-3}, 51% <3 μm).

Table 2 Pigment concentrations at each station determined by HPLC

Station	Z (m)	Chl a (mg m^{-3})	Chlorophyll ratios				Car (mg m^{-3})	PSC ratios			PPC ratios			
			Chl b	Chl c_1	Chl c_2	Mg-DVP		FUCO	VIOLA	PRAS	ALLO	ZEA	DIADINO	LUT
River														
R1	0	0.79	0.05	0.03	0.012	–	0.81	0.52	–	–	0.08	0.16	0.15	0.10
		NS	*NS*	*NS*	*NS*			–			–	–	–	–
R2	0	1.31	0.06	0.04	0.03	–	1.37	0.51	–	–	0.05	0.13	0.21	0.14
		1	*1*	–	–			–			–	–	–	–
	20	1.61	0.06	0.04	0.03	–	1.54	0.51	0.03	–	0.06	0.12	0.17	0.15
		1	*1*	–	–			–	–		–	*5*	–	–
R3	0	1.46	0.07	0.04	0.03	–	1.50	0.51	–	–	0.07	0.13	0.15	0.16
		2	*2*	–	–			–			–	*4*	–	–
	26	0.84	0.07	0.05	0.04	–	0.95	0.56	–	–	0.06	0.16	0.18	0.17
		4	*5*	–	–			–			–	*11*	–	–
R4	0	0.96	0.06	0.02	0.01	–	0.86	0.39	–	–	0.15	0.11	0.10	0.14
		5	*4*		–			–			–	–	–	–
	6	0.56	0.06	0.02	0.01	–	0.92	0.70	–	–	0.18	0.20	0.31	0.25
		6	*5*	–	–			–			–	–	–	–
Esturaine transition zone														
R5d	0	0.73	0.06	0.03	0.02	–	0.86	0.59	–	–	0.13	0.17	0.14	0.15
		7	*12*	–	–			–			–	*17*	–	–
	3.4	1.40	0.06	0.09	0.06	–	1.68	0.60	–	–	0.17	0.06	0.16	0.09
		2	*4*	–	–			–			–	*12*	–	*5*
R5a	0	1.91	0.05	0.04	0.08	0.01	1.65	0.23	–	–	0.35	0.08	0.12	0.06
		20	*28*	*8*	*21*	*21*		–			*29*	*36*	–	–
Shelf														
R6	0	1.02	0.14	0.03	0.07	0.02	0.81	0.18	0.09	0.07	0.27	0.05	0.11	0.04
		20	*30*	*12*	*21*	*26*		–	–	–	*20*	*23*	–	–
R7	0	0.45	0.25	0.03	0.07	0.04	0.22	0.16	0.08	0.10	–	0.09	–	0.05
		61	*66*	*38*	*47*	*62*		*81*	*100*	*98*		–		–
	6.5	0.60	0.05	0.04	0.06	0.01	0.86	0.76	–	–	0.32	0.03	0.28	0.05
		8	*14*		*11*			–			–	–	–	*54*
R8	0	0.24	0.14	0.06	0.25	0.02	0.20	0.39	0.11	–	0.07	–	0.27	–
		45	*69*	*13*	*24*	*40*		*22*	*60*		–		–	
	12	2.20	0.01	0.16	0.30	0.01	3.38	1.36	–	–	0.02	0.01	0.15	–
		4	*17*	*1*	*3*			*2*			–	–	–	
R9	0	0.13	0.17	0.06	0.16	0.02	0.05	0.27	–	–	–	–	–	–
		77	*99*	*40*	*51*	*83*		*34*						
	15	0.52	–	0.19	0.27	0.01	0.74	1.17	–	–	0.08	–	0.18	–
		43			*44*	*100*		*26*			–		–	
	21	0.59	0.01	0.17	0.24	–	0.76	1.02	–	–	0.06	–	0.20	–
		11	–	*4*	*10*			*6*			–		–	

The values in italics for each pigment give the % in the picoplankton fraction (<3 μm). The chlorophyll and carotenoids ratios are expressed relative to Chl *a*. The carotenoids were separated into functional groups: photosynthetic carotenoids (PSC) and photoprotective carotenoids (PPC)

Pigment abbreviations (according to SeaWiFS convention, Werdell and Bailey 2005): *Mg-DVP* magnesium-2,4-divinyl pheoporphyrin a5, *PSC FUCO* fucoxanthin, *VIOLA* violaxanthin, *PRAS* like-prasinoxanthin. PPC: *ALLO* alloxanthin, *ZEA* zeaxanthin, *DIADINO* diadinoxanthin, *LUT* lutein, *NS* not sampled

- Not detected

The carotenoids were regrouped by function into photosynthetic carotenoids (PSC) and photoprotective carotenoids (PPC) as in Trees et al. (2000) and Bricaud et al. (2004). The PSC/PPC pigments ratio from R1 to R3 averaged 0.98 ± 0.04, dropping to 0.76 ± 0.01 at R4. Station R5d had ratios close to those in the river (1.1 ± 0.1) while much lower ratios were measured at R5a (0.38) and R6 (0.51). Over the shelf, the index values at R7 mean of 1.15 ± 0.04 were similar to those in the river while at R8 and R9 there were clear differences with depth; both surface ratio values were around 1.1 ± 0.1 while the deep values for station R8 12 m were 7.8 and an average of 4.3 ± 0.5 for station R9 15 m and 21 m. For the overall data set, these ratios correlated with CDOM concentrations ($r = 0.60$; $df = 18$; $F = 9.61$; $P = 0.007$) but not with turbidity ($r = 0.25$; $df = 19$; $F = 1.21$; $P = 0.29$). A multiple linear regression with both independent variables did not increase the goodness-of-fit beyond that obtained by CDOM alone ($r = 0.60$; $df = 18$; $F = 4.57$; $P = 0.03$).

Primary production

Surface maximum photosynthetic rates (P^*_{max}) were highest in the river, dropping from 9.2 mg C (mg Chl *a* h)$^{-1}$ at R2 to 2.9 mg C (mg Chl *a* h)$^{-1}$ at R8 (Table 3). For the near-surface samples, P^*_{max} was correlated with temperature ($r = 0.89$, $df = 7$, $P = 0.008$) but was not related to CDOM concentrations ($r = 0.57$, $df = 7$, $P = 0.18$). For the entire data set, P^*_{max} was uncorrelated with either temperature ($r = 0.4$; $df = 9$; $P = 0.29$) or a_{320} ($r = 0.14$; $df = 9$; $P = 0.72$), but there was a significant positive correlation with NO_3^- ($r = 0.80$; $df = 9$; $P = 0.009$).

The light utilization coefficient (α) was generally >0.01 (mg C (mg Chl a h)$^{-1}$ (μmol photons m^{-2} s^{-1})$^{-1}$ (Table 3). In the river, α values were around 0.06, decreasing slightly in the estuary, while over the shelf α values were consistently higher in the deep samples. The photoinhibition parameter (β) was generally small in the river, with the exception of R4 where there was the transect maximum of 0.015 mg C (mg Chl *a* h)$^{-1}$ (μmol photons m^{-2} s^{-1})$^{-1}$. Values in the estuary were around 0.0042, dropping lower to 0.0005 over the shelf. The deep sample at R9 was more sensitive to light that the surface samples, with a value of 0.0024 [mg C (mg Chl *a* h^{-1})] (μmol photons m^{-2} s^{-1})$^{-1}$ (Table 3). The light saturation index (E_k) was highest at river station R1, dropping to lower values offshore.

Maximum photosynthetic rates in the surface waters ranged from 2.9 mg C (mg Chl *a* h)$^{-1}$ at station R8 to 9.2 mg C (mg Chl *a* h)$^{-1}$ at R2. P^*_{max} values were high in the deep marine samples, with a maximum of 9.7 mg C (mg Chl *a* h)$^{-1}$ at R8. Primary production rates (PPR) and also integrated daily primary production (PP_{daily}) were highly variable in the river. The lowest PPR value was found at R4 (4.5 mg C m^{-3} h^{-1}) and the minimum daily integrated value for the entire transect was 11.7 mg C m^{-2} day^{-1} at R1 (Table 3). The R5d station had daily primary production rates towards the low end of the range for the river, while both shelf stations had much higher values, with the transect maximum of 455 mg C m^{-2} day^{-1} at R8.

Discussion

The stations sampled across the ARDEX transect clustered into three distinct groups: freshwater river stations (R1–R4),

Table 3 Photosynthetic parameters measured at the ARDEX stations

Station	*Z* (m)	P^*_{max}	α	β	E_k	PPR	PP_{daily}
River							
R1	0	7.2	0.0098	0.0002	733.1	5.7	12.0
R2	0	9.2	0.0629	0.0001	145.8	13.4	143.1
R3	0	5.6	0.0974	0.0055	57.7	6.5	59.0
R4	0	5.9	0.0610	0.0147	96.7	4.5	20.6
Estuarine transition zone							
R5d	0	3.2	0.0464	0.0042	68.1	3.7	36.3
Shelf							
R8	0	2.9	0.0393	0.0007	73.1	0.7	466.8
	12	4.6	0.0904	0.0001	50.6	10.1	
R9	0	4.0	0.0263	0.0005	150.6	0.5	144.7
	21	9.7	0.0759	0.0024	128.1	5.7	

Depth of sampling; maximum photosynthetic rate [P^*_{max} in mg C (mg Chl *a* h)$^{-1}$]; initial slope (α) and photoinhibition parameter (β) in mg C (mg Chl *a* h)$^{-1}$) (μmol photons m^{-2} s^{-1})$^{-1}$, the light saturation parameter E_k (μmol photons m^{-2} s^{-1}), primary production rate (PPR) (mg C m^{-3} h^{-1}) and station daily integrated production (PP_{daily}) (mg C m^{-2} day^{-1})

estuarine transition zone (ETZ) stations (R5d–R5a) and offshore shelf stations (R6–R9). Each of these differed greatly in physical characteristics (temperature, stratification and optical variables) as well as in their phytoplankton biomass, community structure and photosynthetic properties.

Mackenzie River

The freshwater reach of the transect was characterized by warm temperatures, well-mixed water columns (despite depths up to 20 m) and highly turbid conditions. The measured temperatures, up to 19°C, reflect the origin of the source waters at warmer southern latitudes, and the long transit time to the sea across the open tundra landscape that allows considerable sunlight exposure and warming. Similarly warm downstream temperatures have been recorded in Siberian arctic rivers, for example up to 18°C in July–August in the Lena River (Yang et al. 2002). These temperatures are likely to stimulate water column respiration (R) rather than photosynthesis (P) given the severe light limitation for primary production in the river (see below), and will be a factor driving the system towards a negative P/R balance and net heterotrophy.

Soluble reactive phosphorus (SRP), nitrate (NO_3^-) and silica ($Si(OH)_4$) have been reported to occur in moderate concentrations in the river (Millot et al. 2003) and this was confirmed in a parallel study during the ARDEX transect, with mean values of 0.1 μmol l^{-1} (SRP), 5.5 μmol l^{-1} (NO_3^-) and 60 μmol l^{-1} ($Si(OH)_4$) (Emmerton 2006). These data imply that there would be no severe nutrient constraints on the river plankton, although the high mean N/P ratio may indicate some P limitation. The dissolved DOC/DON ratios, averaging around 69, are almost identical to those reported for the Lena River (Lobbes et al. 2000; Dittmar and Kattner 2003) and reveal a strong allochthonous influence on the biogeochemical properties of the river.

The Mackenzie River delivers several million tonnes per year of organic matter, mostly as allochthonous materials (Retamal et al. 2007 and references therein), and the present study underscores the importance of these materials for the underwater light regime. The statistical analyses showed that terrigenous dissolved organic matter (CDOM) had a strong influence on PAR and in the river was the primary constituent controlling the underwater attenuation of UVR. The Mackenzie River is characterized by substantial amounts of sediment (more than 100 million tonnes per year) brought in from the surrounding catchments and maintained in suspension in the turbulent and homogeneous flow of the river. Although this high NAP concentration had no statistically significant effect on short wavelength UVR, there was a strong influence of a_{NAP} on underwater PAR, and longer wavelength UVR (380 nm). The spectral absorption curves also show the importance of both CDOM and NAP for PAR absorption in the river, the decreasing importance of NAP offshore and the increased relative importance of CDOM for UVR absorption. The spectral scattering effects of NAP were not addressed in the current study, and likely play a role in PAR as well as long-wavelength UVR attenuation. Overall, our observations are consistent with optical studies on the abundant lakes in the Mackenzie River floodplain that are flushed each year with river water. The underwater PAR regime of these lakes is primarily controlled by suspended sediment during the spring flood, and then through the rest of summer by CDOM (Squires and Lesack 2003).

Irradiance data are sparse for rivers, but our attenuation values (up to 6.5 m^{-1} for K_{dPAR}) reflect the high sediment load and fall well above those of temperate latitude rivers, for example K_{dPAR} values of 1.8–3.3 m^{-1} in the Ijssel River (Gons et al. 1998) and 1.1 m^{-1} in the St Lawrence River (Vincent et al. 1994). Even in the turbid Yenisei River, vertical attenuation was less than for the Mackenzie, with values smaller than 1.7 (Burenkov et al. 1995). UVR attenuation was also extreme in the Mackenzie River, with K_{d320} values up to 37.04 m^{-1}, well above estimates for the St Lawrence River (1.4 m^{-1}; Scully et al. 2000) and estuary (2 m^{-1}; Kuhn et al. 1999). Previous modelling studies have drawn attention to the pre-eminent importance of CDOM in attenuating UV radiation in northern waters (Gibson et al. 2000; Pienitz and Vincent 2000), and our results show that this conclusion holds for short wavelength UVR even in the presence of large quantities of non-algal particles.

Phytoplankton Chl a concentrations were around 1 mg m^{-3}, similar to previous values for the Mackenzie River (Fee et al. 1988; Garneau et al. 2006). These values are also comparable with those reported for the Great Whale River in eastern subarctic Canada (1.2–1.6 mg Chl a m^{-3}; Rae and Vincent 1998). However, Chl a concentrations were low by comparison with nutrient-enriched large rivers in the temperate zone (up to 11.9 mg Chl a m^{-3} in the St Lawrence River; Vincent et al. 1994), and also relative to Siberian rivers (up to 4.5 mg m^{-3} in the Lena and up to 18.8 mg m^{-3} in the Ob and Yenisei Rivers; Vedernikov et al. 1995; Tuschling 2000). The Mackenzie values are in keeping with a moderate nutrient regime, and may also reflect slow growth relative to loss processes as seen in other turbid rivers (Reynolds et al. 1994). In general, the underwater attenuation of light in large rivers results in a high ratio of mixing depth to euphotic depth that can cause light limitation of phytoplankton production (Reynolds et al. 1994).

The pigment analysis of the river phytoplankton showed that it was largely composed of cells >3 μm. Diatom

pigments were found to be the dominant signature at station R1; this algal group also occurs in high abundance in the Lena River (Tuschling 2000), as well as in the turbulent waters of large temperate rivers; e.g., in the St Lawrence River (Roy et al. 1996). Chlorophyte pigments were also well represented in our Mackenzie River samples, as found in the Yenisei (Matishov et al. 2001) but not Lena River, where picocyanobacteria were the second most dominant group after diatoms (Sorokin and Sorokin 1996). Picocyanobacteria have been recorded as another major constituent of the phytoplankton in rivers elsewhere including the St Lawrence River (Vincent et al. 1994) and the Great Whale River (Rae and Vincent 1998). Although our pigment analysis suggest a low contribution of this fraction in the river, these small cells were also detected by fluorescence microscopy in our ARDEX river sampling, however many of the chroococcoid cells were clustered in colonies that would not pass a 3 μm filter (C. Vallières, unpublished data).

The photosynthetic assays showed that the river phytoplankton had relatively high P^*_{max} and low α and β values. This combination implies a bright-light adapted phytoplankton, and seems counterintuitive relative to the dim average light conditions that are experienced by algae during their circulation through a turbid water column. The values are consistent, however, with observations in the maximum turbidity zone of the St Lawrence River, where low α and β values in combination with high P^*_{max} have been interpreted as acclimation towards intermittent exposure to bright light at the surface rather than to the average water column, extreme shade regime (Vincent et al. 1994). Although P^*_{max} values were high (up to 9.17 mg C (mg Chl *a* h)$^{-1}$, and well above those found in the eastern Subarctic (2.9–3.1; Rae and Vincent 1998), the overall water column production was low (11.7–142.1 mg C m^{-2} day^{-1}) because of the extreme PAR attenuation. The maximum value is comparable with 180 mg C m^{-2} day^{-1} measured in the Lena River (Sorokin and Sorokin 1996), and the range encompasses the values reported for the surface freshwaters of Yenisei bay (79.7–86.6 mg C m^{-2} day^{-1}; Vedernikov et al. 1995).

Estuarine transition zone

There were abrupt changes in all physical properties of the Mackenzie River across its transition zone, and especially in the optical regime. Temperatures dropped to 14°C with the entrainment of cold seawater and the water columns were stratified despite the relatively shallow maximum depths (<4 m). Nutrient concentrations were still moderate as inside the river but with a slight, still non-limiting, decrease in nitrate (3.5 μmol l^{-1}) and SRP (0.05 μmol l^{-1}) (Emmerton 2006). Turbidity dropped substantially (69%) between the upstream and downstream estuarine station, indicating major loss of particles by sedimentation. The particle trapping effect of marine deltas is well known, and studies in the Mackenzie delta have shown that about 50% of the total sediment load is deposited on the bottom as the river water traverses this region (Macdonald et al. 1998). This effect has also been observed in the Siberian river deltas, with loss of 60 to 90% of river-borne particulates by sediment deposition (Vetrov and Romankevich 2004). Despite this loss of sediment, however, the dominant control on the attenuation of PAR throughout the transition zone continued to be a_{NAP}, accompanied by the usual controlling effect of a_{CDOM} on penetration of blue light and UV radiation. The K_{dPAR} values (2–5 m^{-1}) were higher than estuarine transition zones elsewhere, indicating incomplete loss of particles from the sediment laden waters. Much lower values have been recorded in the maximum turbidity zone of the St Lawrence River estuarine transition zone (Vincent et al. 1994), however K_{dPAR} values up to 10 m^{-1} have been recorded in the Yenisei estuary (Burenkov et al. 1995). For the Lena River delta, K_{dPAR} (estimated from Z_{eu}) is much lower, in the range 0.9–1.5 m^{-1} (Sorokin and Sorokin 1996). All of these values, including those for the Mackenzie River system, are likely to be higher under peak discharge conditions.

The highest surface water Chl *a* values for the transect were recorded at station R5a, implying entrainment of nutrients into this frontal region, despite the stratification. The dissolved DOC/DON ratio in the transition zone (32.5) was similar to the Lena River delta (Cauwet and Sidorov 1996), indicative of similar catchment characteristics. Both systems differ substantially from the Yenisei River in terms of this ratio (69.1; Lobbes et al. 2000). The phytoplankton standing stocks in the estuary were similar to those in the river upstream. Our measured values (around 1 mg Chl *a* m^{-3}) fall within the range reported in previous studies in this coastal region (Parsons et al. 1988), and are below the concentrations reported in the estuarine deltas of the North East Lena (1.5–4.5 mg Chl *a* m^{-3}; Heiskanen and Keck 1996), the Yenisei (2.0–5.2 mg Chl *a* m^{-3}) and the Ob (1.6–21.0 mg Chl *a* m^{-3}; Vedernikov et al. 1995), consistent with the higher algal biomass stocks in their inflowing rivers.

The phytoplankton pigment composition in the Mackenzie ETZ also resembled that in the river, with the dominant portion in the larger cell (>3 μm) fraction. There was evidence of increased cryptophytes and a decreased contribution of chlorophytes. In this respect, the Mackenzie estuary seems to differ from those associated with the Ob and Yenisei where green algae and dinoflagellates have been reported by microscopic analysis to dominate (Matthiessen et al. 2000), and the Lena delta where the

community is dominated by brackish water diatoms (Heiskanen and Keck 1996). In the Mackenzie ETZ there was also a clear change in the picoplankton dominance, from 7 to 20%, suggesting more favourable environmental condition for smaller cells (Table 2).

Despite a Chl *a* biomass similar to upstream stations, the transition zone phytoplankton community had much greater integral photosynthetic rates because of the deeper penetration of underwater light. Our estimate of 3.7 mg C m^{-3} h^{-1} at R5d is similar to the values obtained in 1986, of around 5 mg C m^{-3} h^{-1} (Parsons et al. 1988). The integrated daily production rate for the Mackenzie ETZ station (28.3 mg C m^{-2} day^{-1}) is less than one third the values reported for the Siberian systems, for example 107–312 mg C m^{-2} day^{-1} in the Yenisei estuary (Vedernikov et al. 1995) and 100–300 mg C m^{-2} d^{-1} in the Lena delta (Sorokin and Sorokin 1996), consistent with their higher Chl *a*.

Offshore waters over the Mackenzie Shelf

Temperatures were further reduced offshore, but the surface waters remained >5°C even at station R9, indicating the ongoing effect of heat advection from the inflowing river. The underlying water had temperatures and salinities characteristic of the outer shelf (Carmack et al. 2004). Nitrate concentrations in the surface waters at these sites dropped well below those in the river, to an average of 0.1 μmol NO_3^- l^{-1} while SRP rose to higher values, averaging 0.2 μmol l^{-1} (Emmerton 2006). These increased SRP concentrations offshore are common in other coastal systems, including in the Arctic, for example the Yenisei River system (Vedernikov et al. 1995). Turbidity and CDOM concentrations were much reduced and PAR penetrated deeply. The K_{dPAR} coefficients were similar to the 0.4–0.8 m^{-1} range found in the Kara Sea off the Yenisei River (Burenkov et al. 1995). These more transparent conditions are conducive to the development of phytoplankton communities deeper in the water column where nutrient supply is greater.

Chlorophyll concentrations were low in the surface water and comparable with offshore oceanic regions as in the Barents Sea where the same chlorophyll distribution structure is found; i.e., low surface concentrations and the presence of a deep Chl *a* maximum (Kögeler and Rey 1999). However, the low pigment stocks contrast with certain coastal sites elsewhere in the Arctic, for example the Chukchi Sea where pronounced blooms take place each year. The surface phytoplankton at our shelf stations were dominated by small cells, a feature that has also been observed in the Laptev Sea (Tuschling 2000) and many other sites, including a seasonal record from the coastal Beaufort Sea (Lovejoy et al. 2007). Recent work has shown that the phytoplankton community of Mackenzie Shelf contains picocyanobacteria, however these appear to be mostly derived from the Mackenzie River, and the dominance of picoeukaryotes (Waleron et al. 2007). Our record of Prasinophyceae pigments in this region is consistent with the dominance by *Micromonas*-like picoprasinophytes (Lovejoy et al. 2007).

The deep maxima also contained larger cells. Similarly, in the Canada Basin of the Arctic Ocean the contribution of picoplankton to the total phytoplankton community dropped from 69% at the surface to 44% in the deep Chl *a* maximum (Lee and Whitledge 2005). The HPLC analysis of our deep maximum samples showed the presence of Chl c_1, c_3 and fucoxanthin implying high concentrations of diatoms, dinoflagellates and/or raphidiophytes. Deep chlorophyll maxima are found throughout the Arctic Ocean, often in the depth range 15–30 m where the halocline of salinities 31.6–32.4 psu separate the nutrient-poor polar mixed layer from nutrient rich deeper waters (Carmack et al. 2004). However the composition of such maxima appears to be variable. Over the Chukchi shelf, the surface community was dominated by small cells including prasinophytes while larger taxa occurred in the subsurface chlorophyll maxima (Hill and Cota 2005), as over the Mackenzie shelf. Similarly, in the Laptev Sea, a deep maximum at 30 m was composed of diatoms (Heiskanen and Keck 1996). A deep maximum at 30 m in the Northwest Passage contained high concentrations of *Micromonas*-like picoprasinophytes (Lovejoy et al. 2007). Some of these differences maybe the result of seasonal changes, but may also reflect differences in methodology.

The relationship between the PSC/PPC pigment ratio and CDOM implies that the quality of underwater irradiance affected the pigment strategies of the algal community. This pigment ratio was often near 1.0 suggesting that the phytoplankton did not trade off internal protection for photosynthetic efficiency, perhaps because of the high rate of mixing and intermittent exposure to inhibitory surface irradiances. The large PSC/PPC increase in the deep chlorophyll maxima was as expected and is indicative of shade acclimation towards an improved light-capturing ability in a low PAR regime (Ston et al. 2002).

The photosynthetic rates at the offshore stations were lowest per unit biomass, indicating nutrient limitation or, for the deep populations, shading effects. However, because of the deep PAR penetration, the average integrated values for the offshore region were much higher than most measurements throughout the rest of the transect. These values are still below the daily estimates for elsewhere on the Beaufort shelf; e.g., 780 mg C m^{-2} day^{-1} in summer 2002 (Hill and Cota 2005). They are also well below values for the highly productive Chukchi shelf

waters, in which 2,570 mg C m^{-2} day^{-1} was measured at the end of July (Hill and Cota 2005). The light efficiency parameter (α) for the deep maxima was 2–3 times higher than the surface water phytoplankton, indicating physiological acclimation towards dim light conditions, consistent with the pigment data. The specific absorption coefficient was smaller in this deep population than the overlying communities, likely indicating the package effect and self-shading within larger cells (Bricaud et al. 2004).

Conclusions

The high sediment load of the Mackenzie River system has a controlling effect on underwater PAR irradiance and therefore on photosynthesis. Although the P^*_{max} values are relatively high, both per unit biomass and per unit volume, the sharp attenuation of light limits the euphotic zone to the very near-surface waters, and integral water column production is therefore small. CDOM is also a contributing attenuator of PAR, and it is the dominant control on short wavelength UVR through the system. The decrease in sediment load and also CDOM across the transition zone results in improved light availability for photosynthesis, but nutrient supply to the surface waters is restricted by the strong water column stability associated with the pronounced halocline. The highest integral production takes place over the shelf where the concentration of optically active materials is much reduced and PAR penetrates deeply. This allows the development of a deep chlorophyll maximum that can exploit nutrient resources at and below the pycnocline.

Increased permafrost thawing and runoff in the future associated with climate change (ACIA 2005) has the potential to increase the concentrations of CDOM and non-algal particles in large arctic rivers and their coupled marine ecosystems. This in turn could impair photosynthesis in the light-limited algal populations of the river and coastal seas. Increased freshwater runoff to the shelf environment could result in stronger stratification, increased CDOM and NAP shading of phytoplankton in the deep Chl *a* maximum, and may intensify the nutrient limitation of surface populations (Lee and Whitledge 2005) because of reduced vertical transport. The spring bloom period associated with ice algae or phytoplankton production might also be reduced because of earlier depletion of surface nutrients. Offset against this effect, there may be an increased delivery of nutrients with increased runoff (see data for DOC and trace metals in Rember and Trefry 2004), which could delay the depletion of surface nutrients during the open water period. A warmer water column would potentially lead to an increase in P^*_{max} but nutrient supply and light availability would still be the overriding controls on the vertical distribution and daily rates of primary production. All of these conditions would tend to reduce photosynthetic CO_2 fixation, and shift the coastal ecosystem towards a net positive efflux of CO_2 rather than net sequestration into phytoplankton biomass.

Acknowledgments This study was undertaken within ARDEX (Arctic River Delta Experiment), a satellite program of CASES (Canada Arctic Shelf Exchange Study), funded by the Natural Sciences and Engineering Research Council of Canada and the Canada Research Chair program. Financial support was also provided by the Fonds québécois de recherche sur la nature et les technologies and by the Indian and Northern Affairs Canada. We thank Craig Emmerton and Lance Lesack for discussions and for the use of their unpublished nutrient data. We thank Milla Ratio for field support, Marie-Josée Martineau for HPLC technical assistance, and Christine Martineau for her laboratory support. We thank the officers and crew of CCGS Nahidik and our colleagues on the ARDEX program. We also thank the three anonymous reviewers for their insightful comments and suggestions.

References

ACIA (2005) Arctic climate impact assessment. Cambridge University Press, New York

Babin M, Therriault JC, Legendre L, Condal A (1993) Variations in the specific absorption coefficient for natural phytoplankton assemblages: impact on estimates of primary production. Limnol Oceanogr 38:154–177

Belzile C, Vincent WF, Gibson JAE (2002) Colored dissolved organic matter and dissolved organic carbon exclusion from lake ice: implications for irradiance transmission and carbon cycling. Limnol Oceanogr 47:1283–1293

Bricaud A, Babin M, Morel A, Claustre H (1995) Variability in the chlorophyll-specific absorption coefficients of natural phytoplankton: analysis and parameterization. J Geophy Res 100:13,321–13,332

Bricaud A, Claustre H, Ras J, Oubelkheir K (2004) Natural variability of phytoplanktonic absorption in oceanic waters: influence of the size structure of algal populations. J Geophys Res DOI 10.1029/2004JC002419

Burenkov VI, Gol'din YA, Gureev BA, Sud'bin AI (1995) The basic notions of distribution of optical water properties in the Kara Sea. Oceanology 35:346–357

Carmack EC, MacDonald RW (2002) Oceanography of the Canadian Shelf of the Beaufort Sea: a setting for marine life. Arctic 55:29–45

Carmack EC, Macdonald RW, Jasper S (2004) Phytoplankton productivity on the Canadian Shelf of the Beaufort Sea. Mar Ecol Prog Ser 277:37–50

Cauwet G, Sidorov I (1996) The biogeochemistry of Lena River: organic carbon and nutrients distribution. Mar Chem 53:211–227

Dittmar T, Kattner G (2003) The biogeochemistry of the river and shelf ecosystem of the Arctic Ocean: a review. Mar Chem 83:103–120

Droppo IG, Jeffries D, Jaskot C, Backus S (1998) The prevalence of freshwater flocculation in cold regions: a case study from the Mackenzie River Delta, Northwest Territories, Canada. Arctic 51:155–164

Emmerton C (2006) Downstream nutrient changes through the Mackenzie River delta and estuary, Western Canadian Arctic. M.Sc. thesis, Simon Fraser University, Vancouver, BC, Canada

Fee EJ, Hecky RE, Guildford SJ, Anema C, Mathew D, Hallard K (1988) Phytoplankton primary production and related

limnological data for lakes and channels in the Mackenzie Delta and lakes on the Tuktoyaktuk peninsula, N.W.T. Can Tech Rep Fish Aquat Sci 1614, Central and Arctic Region, Department of Fisheries and Oceans, Winnipeg, Manitoba

Ficek D, Kaczmarek S, Stoń-Egiert J, Woźniak B, Majchrowski R, Dera J (2004) Spectra of light absorption by phytoplankton pigments in the Baltic; conclusions to be drawn from a Gaussian analysis of empirical data. Oceanologia 46:533–555

Garneau ME, Vincent FW, Alonso-Sáez L, Gratton Y, Lovejoy C (2006) Prokaryotic community structure and heterotrophic production in a river-influenced coastal arctic ecosystem. Aquat Microb Ecol 42:27–40

Gibson JA, Pienitz R, Vincent WF, Nieke B (2000) Control of biological exposure to UV radiation in the Arctic Ocean: comparison of the roles of ozone and riverine dissolved organic matter. Arctic 53:372–382

Gons HJ, Ebert J, Kromkamp J (1998) Optical teledetection of the vertical attenuation coefficient for downward quantum irradiance of photosynthetically available radiation in turbid inland waters. Aquat Ecol 31:299–311

Gosselin M, Levasseur M, Wheeler PA, Horner RA, Booth BC (1997) New measurements of phytoplankton and ice algal production in the Arctic Ocean. Deep Sea Res Part II 44:1623–1644

Heiskanen AS, Keck A (1996) Distribution and sinking rates of phytoplankton, detritus, and particulate biogenic silica in the Laptev Sea and Lena River (Arctic Siberia). Mar Chem 53:229–245

Hill V, Cota G (2005) Spatial patterns of primary production on the shelf, slope and basin of the Western Arctic in 2002. Deep Sea Res Part II 52:3344–3354

Kishino MN, Takahashi NO, Ichimura S (1985) Estimation of the spectral absorption coefficients of phytoplankton in the sea. Bull Mar Sci 37:634–642

Knap A, Michaels A, Close A, Ducklow H, Dickson A (eds) (1996) Protocols for the Joint Global Ocean Flux Study (JGOFS) core measurements. Bergen, Norway

Kögeler J, Rey F (1999) Ocean colour and the spatial and seasonal distribution of phytoplankton in the Barents Sea. Int J Remote Sens 20:1303–1318

Kuhn P, Browman H, McArthur B, St-Pierre JF (1999) Penetration of ultraviolet radiation in the waters of the estuary and Gulf of St. Lawrence. Limnol Oceanogr 44:710–716

Lee SH, Whitledge TE (2005) Primary and new production in the deep Canada Basin during summer 2002. Polar Biol 28:190–197

Lobbes JM, Fitznar HP, Kattner G (2000) Biogeochemical characteristics of dissolved and particulate organic matter in Russian rivers entering the Arctic Ocean. Geochim Cosmochim Acta 64:2973–2983

Lovejoy C, Vincent WF, Bonilla S, Roy S, Martineau MJ, Terrado R, Potvin M, Massana R, Pedrós-Alió C (2007) Distribution, phylogeny and growth of cold-adapted picoprasinophytes in arctic seas. J Phycol 43:78–89

Macdonald RW, Solomon SM, Cranston RE, Welch HE, Yunker MB, Gobeil C (1998) A sediment and organic carbon budget for the Canadian Beaufort Shelf. Mar Geol 144:255–273

Manson G, Solomon S, MacDonald A (2001) Arctic coastal dynamics: describing Beaufort Sea coastal climate variability. Extended Abstract, International Arctic Sciences Committee (IASC) and the International Permafrost Association, Potsdam, Germany

Matishov GG, Druzhkov NV, Makarevich PR, Larionov VV (2001) The role of freshwater phytoplankton in formation of the enhanced productivity region in the Ob-Yenisei shallow waters. Dokl Biol Sci 378:251–253

Matthiessen J, Kunz-Pirrung M, Mudie PJ (2000) Freshwater chlorophycean algae in recent marine sediments of the Beaufort, Laptev and Kara Seas (Arctic Ocean) as indicators of river runoff. Int J Earth Sci 89:470–485

Millot R, Gaillardet J, Dupré B, Allegre CJ (2003) Northern latitude chemical weathering rates: clues from the Mackenzie River Basin, Canada. Geochim Cosmochim Acta 67:1305–1329

Mitchell BG, Kahru M, Wieland J, Stramska M (2003) Determination of spectral absorption coefficients of particles, dissolved material and phytoplankton for discrete water samples. In: Mueller JL, Fargion GS, McClain CR (eds) Ocean optics protocols for satellite ocean color sensor validation, Revision 4, vol IV: Inherent optical properties: instruments, characterizations, field measurements and data analysis protocols. NASA Technical Memorandum TM-2003-211621/R, Goddard Space Center, Greenbelt, MD pp 39–64

Oke TR (1988) Boundary layer climates. Taylor & Francis Group, London

Parsons TR, Webb DG, Dovey H, Haigh R, Lawrence M, Hopky GE (1988) Production studies in the Mackenzie River Beaufort Sea estuary. Polar Biol 8:235–239

Pienitz R, Vincent WF (2000) Effect of climate change relative to ozone depletion on UV exposure in subarctic lakes. Nature 404:484–487

Platt T, Gallegos CL, Harrison WG (1980) Photoinhibition of photosynthesis in natural assemblages of marine phytoplankton. J Mar Res 38:687–701

Platt T, Harrison WG, Horne EPW, Irwin B (1987) Carbon fixation and oxygen evolution by phytoplankton in the Canadian high arctic. Polar Biol 8:103–113

Pullin MJ, Cabaniss SE (1995) Rank analysis of the pH-dependent synchronous fluorescence spectra of six humic substances. Environ Sci Technol 29:1460–1467

Rae R, Vincent WF (1998) Phytoplankton production in subarctic lake and river ecosystems: development of a photosynthesis–temperature-irradiance model. J Plankton Res 20:1293–1312

Rember RD, Trefry JH (2004) Increased concentrations of dissolved trace metals and organic carbon during snowmelt in rivers of the Alaskan Arctic. Geochim Cosmochim Acta 68:477–489

Retamal L, Vincent WF, Martineau C, Osburn CL (2007) Comparison of the optical properties of dissolved organic matter in two river-influenced coastal regions of the Canadian Arctic. Estuar Coast Shelf Sci 72:261–272

Reynolds CS, Descy JP, Padisák J (1994) Are phytoplankton dynamics in rivers so different from those in shallow lakes? Hydrobiologia 289:9–21

RNC (2003) L'Atlas du Canada:Pergélisol. Ressources Naturelles Canada

Roy S, Chanut JP, Gosselin M, Sime-Ngando T (1996) Characterization of phytoplankton communities in the lower St. Lawrence Estuary using HPLC-detected pigments and cell microscopy. Mar Ecol Prog Ser 142:55–73

Scully N, Vincent WF, Lean D (2000) Exposure to ultraviolet radiation in aquatic ecosystems: estimates of mixing rate in Lake Ontario and the St. Lawrence River. Can J Fish Aquat Sci 57:43–51

Sharp JH, Benner R, Bennett L, Carlson CA, Dow R, Fitzwater SE (1993) Re-evaluation of high temperature combustion and chemical oxidation measurements of dissolved organic carbon in seawater. Limnol Oceanogr 38:1774–1782

Sorokin YI, Sorokin PY (1996) Plankton and primary production in the Lena River estuary and in the south-eastern Laptev Sea. Estuar Coast Shelf Sci 43:399–418

Squires MM, Lesack LFW (2003) Spatial and temporal patterns of light attenuation among lakes of the Mackenzie Delta. Freshw Biol 48:1–20

Ston J, Kosakowska A, Lotocka M, Lysiak-Pastuszak E (2002) Pigment composition in relation to phytoplankton community

structure and nutrient content in the Baltic Sea. Oceanologia 44:419–437

Telang SA, Pocklington R, Naidu AS, Romankevich EA, Gitelson II, Gladyshev MI (1991) Carbon and mineral transport in major North American, Russian Arctic, and Siberian rivers: the St-Lawrence, the Mackenzie, the Yukon, the Arctic Alaskan Rivers, the Arctic Basin rivers in the Soviet Union, and the Yenisei. In: Degens E, Kempe S, Richey J (eds) SCOPE 42 biogeochemistry of major world rivers. Wiley, London, pp 75–104

Trees CC, Clark DK, Bidigare RR, Ondrusek ME, Mueller JL (2000) Accessory pigments versus chlorophyll *a* concentrations within the euphotic zone: a ubiquitous relationship. Limnol Oceanogr 45:1130–1143

Trefry JH, Rember RD, Trocine RP (2005) Sources, concentrations and dispersion pathways for suspended sediment in the coastal Beaufort Sea—executive summary. OCS Study MMS 2005-051 U.S. Department of the Interior Minerals Management Service, pp 28–31

Tuschling K (2000) Phytoplankton ecology in the arctic Laptev Sea-comparison of three seasons. Ber Polarforsch 347:1–3

Vedernikov VI, Deminov AB, Sud'bin AI (1995) Primary production and chlorophyll in the Kara Sea in September. Oceanology 34:630–640

Vetrov AA, Romankevich EA (eds) (2004) Horizontal carbon fluxes in the land-sea system. In: Carbon cycle on the Russian Arctic Seas. Springer, Berlin, pp 201–227

Vincent WF, Bertrand N, Frenette JJ (1994) Photoadaptation to intermittent light across the St. Lawrence estuary freshwater–saltwater transition zone. Mar Ecol Prog Ser 110:283–292

Waleron M, Waleron K, Vincent WF, Wilmotte A (2007) Allochthonous inputs of riverine picocyanobacteria to coastal waters in the Arctic Ocean. FEMS Microbiol Ecol 59:356–365

Wehr JD, Descy JP (1998) Use of phytoplankton in large river management. J Phycol 34:741–749

Werdell PJ, Bailey SW (2002) The SeaWiFS bio-optical archive and storagesSystem (SeaBASS): current architecture and implementation. NASA technical memorandum, NASA/TM-2002–211617, Goddard Space Center, Greenbelt, MD

WRI (2003) Water Resources eAtlas–Watershed of North and Central America, NA08 Mackenzie. IUCN, IWMI, Rasmar Convention Bureau and WRI

Yang D, Kane DL, Hinzman LD, Zhang X, Zhang T, Hengchun Y (2002) Siberian Lena River hydrologic regime and recent change. J Geophys Res 107:4694–4704

Yunker MB, Macdonald RW, Veltkamp DJ, Cretney WJ (1995) Terrestrial and marine biomarkers in a seasonally ice-covered Arctic estuary—integration of multivariate and biomarker approches. Mar Chem 49:1–50

Zapata M, Rodriguez F, Garrido JL (2000) Separation of chlorophylls and carotenoids from marine phytoplankton: a new HPLC method using a reversed phase C8 column and pyridine containing mobile phases. Mar Ecol Prog Ser 195:29–45